THE EFFECTS OF ONCOGENIC G12D MUTATION ON K-RAS STRUCTURE, CONFORMATION AND DYNAMICS

Sezen Vatansever[1, 2, 3], Zeynep H. Gümüş[2, 3]*, Burak Erman[1]*

[1]Department of Chemical and Biological Engineering, College of Engineering, Koç University, Rumelifeneri Yolu, 34450, Sarıyer, Istanbul, Turkey
[2]Department of Genetics and Genomics, [3]Icahn Institute for Genomics and Multiscale Biology, Icahn School of Medicine at Mount Sinai, New York, NY 10029

*Correspondence: berman@ku.edu.tr (B.E.) and zeynep.gumus@mssm.edu (Z.H.G.)

ABSTRACT

K-Ras is the most frequently mutated protein in human tumors. Activating K-Ras mutations drive cancer initiation, progression and drug resistance, directly leading to nearly a million deaths per year. To understand the mechanisms by which mutations alter K-Ras function, we need to understand their effects on protein dynamics. However, despite decades of research, how oncogenic mutations in K-Ras alter its conformation and dynamics remain to be understood. Here, we present how the most recurrent K-Ras oncogenic mutation, G12D, leads to structural, conformational and dynamical changes that lead to constitutively active K-Ras. We have developed a new integrated MD simulation data analysis approach to quantify such changes in a protein and applied it to K-Ras. Our results show that G12D mutation induces strong negative correlations between the fluctuations of SII and those of the P-loop, Switch I (SI) and α3 regions in K-Ras^{G12D}. Furthermore, characteristic decay times of SII fluctuations significantly increase after G12D mutation. We have further identified causal relationships between correlated residue pairs in K-Ras^{G12D} and show that the correlated motions in K-Ras dynamics are driven by SII fluctuations, which have the strongest negative correlations with other protein parts and the longest characteristic decay times in mutant K-Ras. Ours is arguably the first study that shows the causal relationships between residue pairs in K-Ras^{G12D}, relates them to the decay times and correlates their fluctuations.

Keywords: K-Ras, KRAS, causality, time-delayed correlation, molecular dynamics

INTRODUCTION

K-Ras is the most frequently mutated oncoprotein in human cancers[1-3]. Patients with oncogenic K-Ras mutations have very poor response to standard therapies. Unfortunately, K-Ras mutations eventually emerge during the course of their treatment and drive acquired resistance[4-6]. K-Ras functions as a small GTPase and is critical in the regulation of intracellular signaling networks in cellular growth, proliferation and differentiation[7]. To perform its cellular roles, it switches between its inactive GDP-bound and active GTP-bound states[8,9]. Only active K-Ras (K-Ras-GTP) can bind and activate its downstream effector proteins[10]. Active K-Ras catalyzes GTP hydrolysis to become inactive (K-Ras-GDP). Intrinsic GTPase function of active K-Ras can be accelerated by the binding of GTPase-activating proteins (GAPs)[11,12]. However, certain mutations in K-Ras impair its intrinsic GTPase function and GAP binding and thereby GTP hydrolysis. Unable to switch to its GDP-bound inactive state, mutant K-Ras remains continuously active, causing prolonged activation of downstream pathways associated with oncogenic cell growth[10,13-15].

In cancer patients, oncogenic K-Ras mutations are recurrently observed at positions 12, 13 and 61. G12 is the most frequently mutated residue (89%), which most prevalently mutates to aspartate (G12D, 36%) followed by valine (G12V, 23%) and cysteine (G12C, 14%)[3,10]. This residue is located at the protein active site, which consists of a phosphate binding loop (P-loop, residues 10-17) and switch I (SI, residues 25-40) and II (SII, residues 60-74) regions. The active site residues are bound to the phosphate groups of GTP and are responsible for the GTPase function of K-Ras. In its side-chain, G12 has only a single hydrogen. However, the mutation to aspartate (G12D) leads to the projection of a bulkier side group into the active site, which causes a steric hindrance in GTP hydrolysis[16], impairs the GTPase function and locks K-Ras in its active GTP-bound state[12]. There is strong evidence that blocking mutant K-Ras activity can be very effective in the treatment of cancer patients[17,18]. Yet, despite decades of research, there are still no drugs in the clinic today that can directly target mutant K-Ras[19,20]. Although the effects of G12D mutation on the structure, conformation and flexibility of K-Ras have been studied[21-24], the relationship between its conformational and dynamical changes still remains to be understood. At the same time, there is increasing evidence that suggests that crystal structure studies alone may miss drug-binding pockets on mutant K-Ras surface[18,25-33]. Studies that include dynamics information have recently achieved promising results, however, these are limited to K-Ras^{G12C} mutant, and the mechanisms that regulate its dynamics remain unknown. Understanding the mechanisms of dynamic regulation of mutant K-Ras can present novel opportunities for identifying clinically actionable regulatory sites on its surface, making a profound impact in the treatment of millions of patients.

Here, we present an in-depth study of how the most prevalent oncogenic K-Ras mutation, G12D, triggers structural, conformational and dynamic changes in the protein that result in its constitutive activation. Recent studies suggest that utilizing protein dynamics data is a successful approach for understanding the effects of mutations on the structure, dynamics and function of proteins[34-36]. Particularly in drug discovery, dynamics data from oncogenic proteins[22,37-40] have helped identify cryptic or allosteric binding sites[41-44]. We hypothesized that dynamic regulatory mechanisms can best be explored by detailed analyses of their molecular dynamics (MD) simulation data, from which we can predict the regulatory relationships between residue pairs. For this purpose, we developed an integrated MD simulation data analysis approach that uses several computational metrics to quantify

mutation-based changes in protein structure and its consequences. Our approach is based on the conditional time-delayed correlations (CTC) method we have recently developed, which uses time delayed correlation functions from MD datasets to provide information on the correlation of two events, one taking place at time *t* and the other at a later time, $t+\tau$. This approach has been remarkably accurate in predicting sites that control a protein's motions[45], and has shown excellent agreement with experimental data when tested on wild-type K-Ras (K-Ras^{WT}).

We first performed MD-simulations of GTP-bound active forms of both wild type and G12D mutant K-Ras (hereafter K-Ras^{WT} and K-Ras^{G12D}) and applied our CTC method to predict sites on mutant K-Ras^{G12D} surface that control its activity. From the CTC results, we first studied the structural changes in both GTP and GDP-bound K-Ras upon G12D mutation, and discovered salt bridges that are either formed or destroyed upon mutation. Second, we evaluated the changes in the pair-wise distances between residues and quantified the local volume changes to identify changes in protein conformation. Third, we identified changes in protein dynamics through a multi-step process where we (i) quantified the residue fluctuations; (ii) evaluated correlation of residue fluctuations and identified lost or newly formed correlations upon mutation; (iii) calculated the characteristic decay times of residue fluctuations; and (iv) identified residue pairs that are causally related (i.e., residue pairs that show driver-responder behavior). Finally, we related the observed structural changes to the conformational and dynamical alterations, which enabled us to identify the important changes that affect protein function. Overall, our study identifies regulatory sites on K-Ras^{G12D}, which enhance our understanding of its dynamics and can assist in the development of direct inhibitors.

METHODS

MD SIMULATIONS

We performed all-atom MD simulations for both Mg^{+2}GTP-bound K-Ras^{WT} and K-Ras^{G12D}. We obtained the K-Ras-GTP^{WT} structure from the final frame of the 300ns simulation of active state protein by Vatansever *et al*[45]. For constructing K-Ras^{G12D} structure, we mutated glycine to aspartate at position 12 in K-Ras-GTP^{WT} structure using Discovery Studio 4.5 software, (DS)[46]. To optimize the K-Ras^{G12D}-GTP complex, we used Clean Geometry tool of DS. For MD simulations, we used NAMD 2.10[47] with AMBER ff99SB[48] and general amber force fields (GAFF)[49]. Briefly, we performed energy minimization of the initial model after we introduced the G12D mutation in K-Ras, and then ran MD simulations of each complex following the protocols from our previous study[45], the details of which we provide in Supplementary Methods. During the simulations, we applied minimization for 10,000 steps and equilibration for 500,000 steps, after which we performed 1 microsecond MD simulations, and saved atomic coordinates $\hat{R}$ of all atoms every 10ps. we used the last 900ns of the simulation trajectories in all computations described in this study. To eliminate all rotational and translational motions, we aligned the trajectories to the first frame using VMD software 1.9.2[50]. We visualized the trajectories with VMD. To identify salt bridges formed in the protein during the MD simulations, we used Salt Bridges Plugin, Version 1.1, of VMD.

PAIRWISE DISTANCE CALCULATIONS

To quantify the effect of the G12D mutation on the distances between K-Ras residue pairs, we developed a new computational algorithm detailed in Figure S1. Briefly, we first assumed K-Ras^{WT} as the initial state and K-Ras^{G12D} as the final state. Then, we calculated the distances between Cα atoms of two residues (*i*, *j)* as we previously described[45]. A widely used model to analyze protein dynamics is Gaussian network model (GNM). Studies that use GNM typically assume the maximum Cα-Cα distance for the separation between two contacting residues at ~7.2Å[51,52], and label it the 'first coordination shell'[53,54]. We followed this same protocol and determined the first coordination shell around a selected residue by choosing its Cα as the center of a volume V with a radius of r1 ~7.2 Å[52]. However, because the contribution of non-bonded pairs to higher-order coordination shells may also be significant[54,55], we also studied residue pairs that are within their 'second coordination shell' in K-Ras^{WT} structure. We defined this second coordination shell at twice the volume of the first, with a radius of ~9.1 Å[54].

For every residue pair *(i, j)* where *j* is in the second coordination shell of *i*, we first calculated its time-averaged distance in K-Ras^{WT} ($\bar{R}_{ij\ \mathrm{WT}}$) and in K-Ras^{G12D} ($\bar{R}_{ij\ \mathrm{G12D}}$). We then calculated the difference ($\Delta\bar{R}ij$) between $\bar{R}_{ij\ \mathrm{WT}}$ and $\bar{R}_{ij\ \mathrm{G12D}}$, where $\Delta\bar{R}ij = \bar{R}_{ij\ \mathrm{G12D}} - \bar{R}_{ij\ \mathrm{WT}}$. The magnitude of the difference is the degree of distortion resulting from the G12D mutation. We present $\Delta\bar{R}ij$ values in the pairwise distances map (Figure 1) where a positive value indicates that a residue pair moves apart upon G12D mutation, while a negative value indicates that the pair gets closer. Then, we identified the residue pairs (*ij*) significantly distorted by the G12D mutation. For this purpose, we selected the residue pairs that have the greatest (positive and negative) $\Delta\bar{R}ij$ values. We assumed that the residue pairs whose $\Delta\bar{R}ij$ values are greater than 2.75 or smaller than -1.35 showed the most significant distance changes. For those identified residue pairs, we drew the distribution graphs $W(R_{ij})$ of their distances (R_{ij}) during the simulations of K-Ras^{WT} and K-Ras^{G12D} (For details see Supplementary).

Then, to quantify the changes in local volumes upon G12D mutation, for each residue *i* we calculated the average of all $\Delta\bar{R}_{ij}$ values based on the formula $\langle\Delta\bar{R}i\rangle = \sum_j \Delta\bar{R}ij/N_n$, where N_n is the number of residues *j* in the second coordination shell of residue *i*. In detail, for a residue *i*, at the center of a volume V with a radius of 9.1 Å (the second coordination shell) and we defined the residues *j* within this volume V as the *neighbors* of residue *i*. Then, we calculated the total change in the distance between residue *i* and its neighbors,$\sum_j \Delta\bar{R}ij$, and divided it by the number of neighbors $\sum_j \Delta\bar{R}ij/N_n$. The resulting $\langle\Delta\bar{R}i\rangle$ value is a measure of the change in volume around residue *i* due to G12D mutation.

PAIRWISE CORRELATION, TIME DELAYED CORRELATION AND CHARACTERISTIC DECAY TIME CALCULATIONS

To show coupled motions in protein dynamics, we calculated the correlation coefficients between the fluctuations of residue pairs (C_{ij}). A correlation coefficient value of a residue pair ranges from -1 to 1, where for residue pair fluctuations that are not coupled *Cij*= 0; perfectly positively correlated C*ij*=1, and perfectly negatively correlated C*ij*=-1. Additionally, to identify the directionality (causality) in the correlated motions of residue pairs, we calculated the time-delayed correlations between them ($C_{ij}(\tau)$), where τ is the time-delay. $C_{ij}(\tau)$ value represents the degree and manne in which the past fluctuations of residue *i* and the present fluctuations of residue *j* are coupled.

We further calculated autocorrelations $C_{ij}(\tau)$ of each protein residue, which is the coupling of its past and present fluctuations. A slow decay of $C_{ii}(\tau)$ function indicates that the present fluctuations of residue *i* tend to be strongly coupled with its own past fluctuations and thereby that residue *i* has a strong *memory* of its past fluctuations. To measure the memory length for a residue *i,* we calculated the time-delay value (τ) where the autocorrelation decay curve of the residue *i* reaches to 0.5 and we accepted it as the characteristic decay time of the residue *i*. We adopted the 0.5 criterion instead of the commonly used 1/e decay criterion because it was a better indicator of short time relaxation differences while the latter led to values too close to each other.

The the calculations of correlation coefficients, time-delayed correlations and autocorrelations were as described in our previous study[45] and are summarized in detail in Supplementary.

RESULTS

1.Structural Changes

New close-range electrostatic interactions (salt bridges) are formed in K-Ras^{G12D}., which are not present in K-Ras^{WT}. Substitution of a non-polar, non-charged amino acid (glycine) with a negatively-charged amino acid (aspartate) triggers several conformational and dynamical changes in K-Ras^{G12D}. With the plausible assumption that the negatively charged residue D12 may cause new electrostatic interactions within the protein and that those interactions can be the sources of conformational changes upon G12D mutation, we compared the close-range electrostatic interactions (i.e. salt bridges) in K-RAS^{WT} *vs*. K-RAS^{G12D}. In the mutated structure, D12 forms salt bridges with K16 (P-loop) and K88, and K16 forms a salt bridge with D57. However, none of these interactions are present in K-RAS^{WT}. To identify the effects of the new electrostatic interactions caused by G12D mutation, we then investigated the conformational changes in K-Ras.

2.Conformational Changes

Pairwise Distance Calculations show conformational changes in K-Ras^{G12D} vs. K-Ras^{WT}. We compared the distances between residue pairs within *their second coordination shell* in K-Ras^{WT} vs. K-Ras^{G12D}, where *the first coordination shell* is the maximum Cα-Cα distance of the separation between two contacting residues ~7.2Å[51-54] and the *second coordination shell* is twice the volume of the first, at a radius of ~9.1Å[54]. In Figure 1A, we show the $\Delta\bar{R}_{ij}$ values for all residue pairs where K-Ras^{WT} is the reference and K-Ras^{G12D} is the final structure. As seen from the abundance of positive $\Delta\bar{R}_{ij}$ values, the dominant distortion of the protein upon mutation is expansion, where SII region (T58-T74) moves away from the phosphate binding loop (P-loop, G10-S17), SI (Q25-Y40), α3 (T87-K104) in K-Ras^{G12D}. The SI region also moves away from the P-loop. In detail, all the P-loop residues move away from T58-R68 (SII) residues as a block. Second, the residues in the segment P34-Y40 of SI move away from N-terminal residues of SII (D57-Q61). Third, the α2 helix of SII moves away from α3, D92-R102. Fourth, SI residues move away from the P-loop residues. On the other hand, SI residues (F28-Y32, Y32-I36) assume a closer conformation where an H-bond between D33 and I36 is established. This causes the T35-E37 part of SI to move away from the P-loop residues, G13-K16.

We observed the most significant changes in the distances between residue pairs Q61 (SII)-A11 (P-loop), Q61 (SII)-G12D (P-loop), Q61 (SII)-G13 (P-loop), E37(SI)-D57 (SII) and S65 (SII)-H95(α3) (Figure 1B). Residues R68, M72 and Y96 were also further apart in K-Ras^{G12D}. On the other hand, we observed that some residue pairs got significantly closer in K-Ras^{G12D}, including E63-R68, M72-G75 and R73-K104, demonstrated by their negative $\Delta\bar{R}_{ij}$ values in Figure 1A.

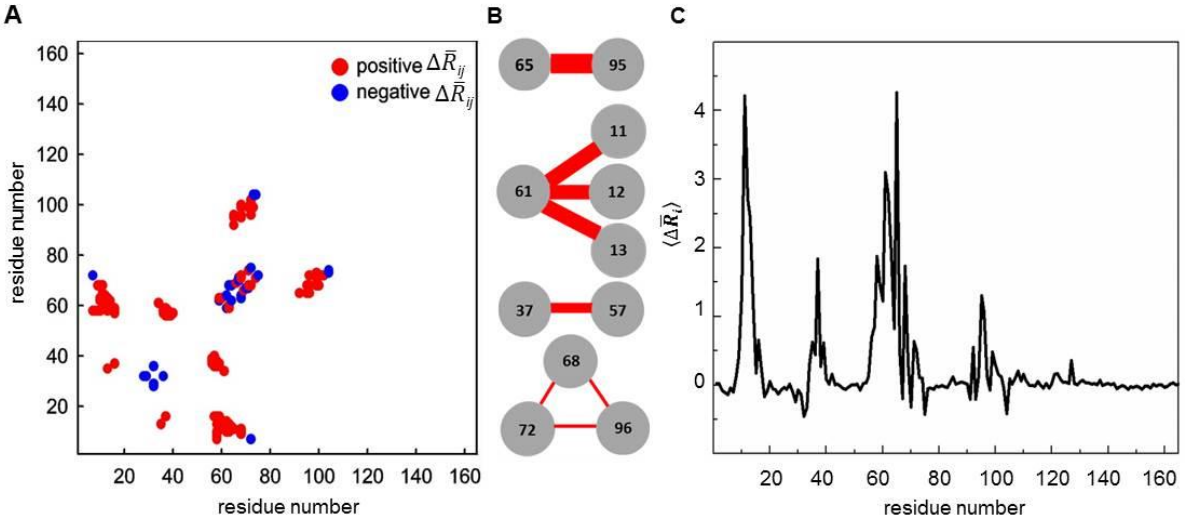

Figure 1. Conformational changes in K-Ras upon G12D mutation. (A) Difference of the average pairwise distances ($\Delta\bar{R}_{ij}$) where K-Ras^{WT} is the initial and K-Ras^{G12D} is the final state. Red dots (positive $\Delta\bar{R}_{ij}$ values) show that pairs move further apart and blue dots (negative $\Delta\bar{R}ij$ values) show that pairs move closer in K-Ras^{G12D}. (B) Scheme for the residue pairs that show the most significant distance changes. Spheres represent the residues; the widths of edges that connect the residue pairs represent the magnitude of the $\Delta\bar{R}ij$ values. (C) The average of all $\Delta\bar{R}_{ij}$ values for each residue, $\langle\Delta\bar{R}i\rangle$. The initial state is K-Ras^{WT} and the final state is K-Ras^{G12D}. The residues which move away from their neighbors have positive values and dominate the mutant protein; residues that move close to their neighbors have negative values.

K-Ras^{G12D} has broader distance distributions than K-Ras^{WT}. To uncover the conformational differences between wild type and mutant K-Ras and to thereby better understand the effects of the G12D mutation, we calculated the probability distributions of the distances between pairs of residues that exhibited the largest changes in the distance calculations. Distance distributions of the residue pairs which underwent the largest changes due to G12D mutation are shown in Figure 2. These are between the alpha carbons of residue pairs A11-Q61, G12D-Q61 and G13-Q61, respectively, as shown in Fig. 2A-C. Their distribution patterns exhibit marked differences between WT and mutant K-Ras. In WT K-Ras, they exhibit a narrow distance distribution with smaller peaks compared to the mutant form. Residues A11, G12 and G13 are located at the P-loop. The P-loop has an omega shape and forms a turn at the C-terminal neighborhood of G12. As shown in Figure 2A-B, A11 and G12 are located within H-bond distance from Q61, while the distance between G13 and Q61 is increased. Furthermore, we observed that in K-Ras^{WT}, G12 (side chain H atom) forms an H-bond with G60 (backbone O atom), the neighbor of G60. However, in K-Ras^{G12D}, this H-bond disappears because of the bulkier side chain of D12. In the absence of this H-

bond, D12 and its neighbors move away from Q61. The broadened distance distribution values of the mutant protein are indicators of lost hydrogen bonds.

In K-Ras^{WT} simulations, we observed an H-bond between D38 (SI) and D57 (SII). However, this H-bond dissappers in K-Ras^{G12D} simulations, leading D57 to move away from D38 and more remarkably from E37. The absence of this H-bond in K-Ras^{G12D} is shown in Figure 2D where the peak distance value is greater in the K-Ras^{G12D}.

Among all residue-residue pairs, S65-H95 undergoes the largest conformational change upon mutation. S65 is on α2 and moves away from H95, which is on α3 in K-Ras^{G12D} (Figure 2E). The simulations show that this significant change due to the brakeage of the salt bridge between α2 and α3 helices. In K-Ras^{WT}, these two helices interact through the salt bridge between R68 and D92. However, the G12D mutation breaks the R68-D92 salt bridge and causes the α2 and α3 helices to move away from each other. This conformation of α2 and α3 in K-Ras^{G12D} can be deduced from Figure 2E, which shows that the distance distribution curve of S65 (α2)-H95 (α3) has a higher peak. Finally, the distances between the residues R68, M72 and Y96 are also more stable in K-Ras^{WT} as shown in Figure 2F-H.

Overall, we observed that distance distribution curves for K-Ras^{WT} are characterized by Gaussian-shaped, narrow dispersion curves. We use the term 'stable' in the sense that the distribution has a sharp peak, with a small dispersion around it. However, mutant K-Ras showed significant deviations from the Gaussian, except for the residue pair E37(SI)-D57 (SII).

We show the distance distributions of the residue pairs which became significantly closer upon mutation in Figure S2. During the MD simulations, E63-R68 pair is in a closer conformation in K-Ras^{G12D} (Figure S2A). This conformation may have resulted from the residues adjacent to E63, Y64 and S65, making H-bonds with R68 and D69, respectively. We observed these H-bonds between the backbone H atoms of Y64 & S65 and the backbone O atoms of R68 & D69 only in K-Ras^{G12D}. Additionally, during the K-Ras^{G12D} simulations R73-K104 pair also assumed a closer conformation which may have resulted from the H-bonds between R73-D105 and G75-K104 (Figure S2B).

On the other hand, in Figure S2C, we show that the residue pair M72-G75 switches between two conformations in K-Ras^{WT}, where one has a closer conformation around 5.5 Å and the other one has a distant conformation around 8.5 Å. However, their distance distribution has a single peak at 5.5 Å in K-Ras^{G12D} that is similar to the closer conformation in K-Ras^{WT}. We have observed that the residue M72 forms an H-bond with G75 only in K-Ras^{G12D}. This H-bond may have caused their single-peaked distance distribution.

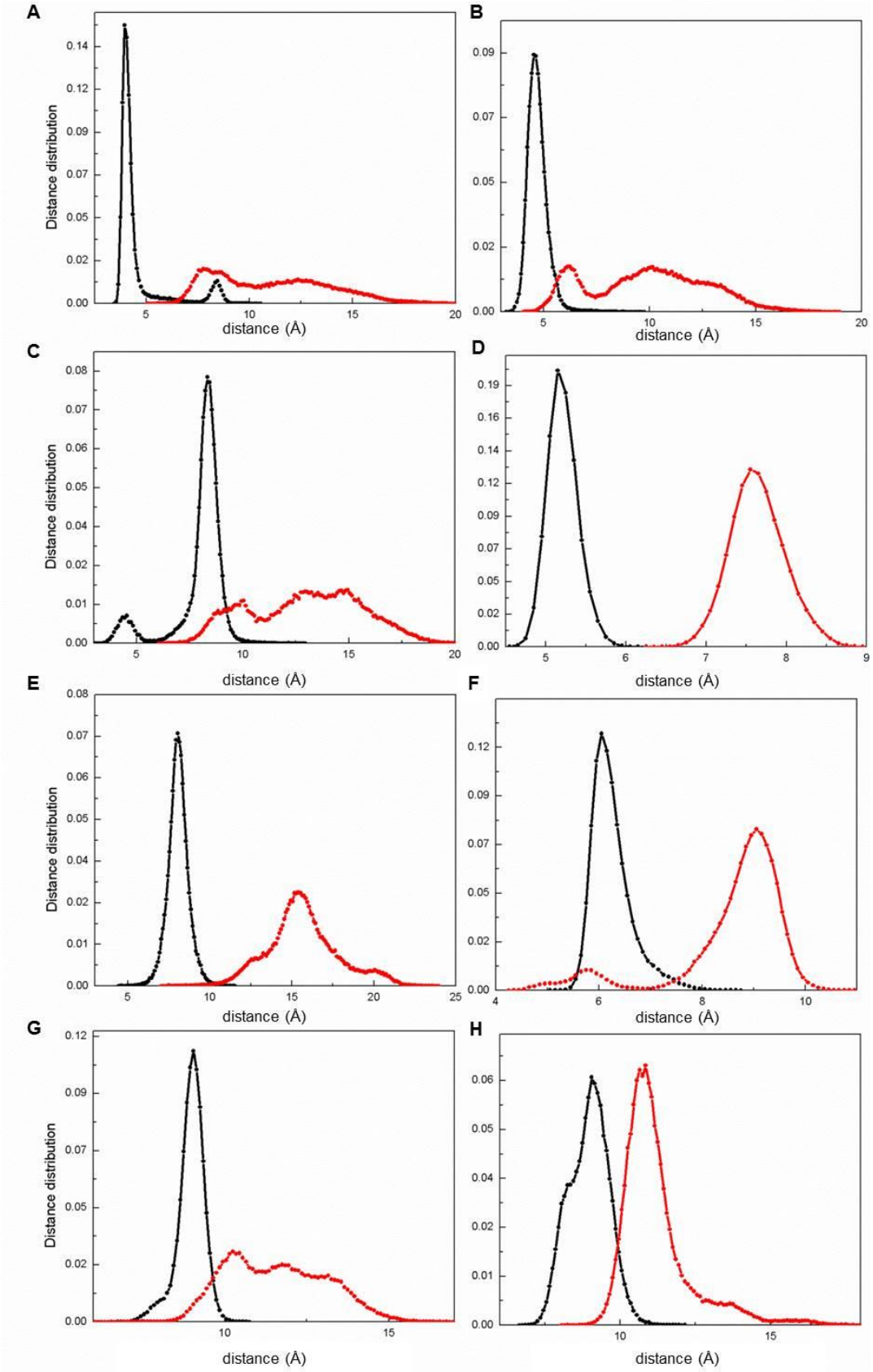

Figure 2. Distribution of distances between residue pairs in K-Ras^{WT} (black) and K-Ras^{G12D} (red). Distance distribution of residue pairs (A) Q61-A11; (B) Q61G-12D; (C) Q61-G13; (D) E37-D57; (E) S65-H95; (F) R68-M72; (G) M72-Y96; (H) R68-Y96.

G12D mutation causes changes in local volume. According to the GNM model, a residue typically fluctuates within its first or second coordination shell[51,52]. Within these fluctuation volumes, there are several other residues, which are either near-neighbors along the chain or are spatially distant. As has been shown by the GNM model, each residue has a different number of neighbors[52]. A residue with a smaller number of neighbors will show larger fluctuations than a residue with a larger number of neighbors. Therefore, the neighborhood of a given residue significantly affects its fluctuations, and as we will show here there is also a significant effect on its dynamics. In order to understand which parts of K-Ras move away from its neighbors and which parts move closer upon mutation, we have calculated the average of all $\Delta\bar{R}_{ij}$ values for each residue, $\langle\Delta\bar{R}i\rangle$. Figure 1C shows that most of the protein parts, especially the P-loop and SII, move away from their neigbors after G12D mutation.

In summary, we identified the residue pairs that underwent the largest distance change due to G12D mutation. In addition, for each residue in the identified pairs, we showed the extent of its deviation from its neighbors. For this purpose, we have compared the individual $\sum_j \Delta\bar{R}ij$ values of the residues in the identified pairs (Table S1). We discovered that the residues which move further away from each other in K-Ras^{G12D} also move away from their neighbors. On the other hand, the residues that move closer to each other in K-Ras^{G12D} have different conformations relative to their neighbors.

3. Dynamic Changes

Residue fluctuations of central residues of SII are increased in K-Ras^{G12D}. To understand how the flexibility of K-Ras changes upon G12D mutation, we calculated the root-mean-square fluctuations (RMSF) of each residue in both wild-type and mutant protein, where RMSF is a measure of the average atomic fluctuations of a residue. In Figure 3A, we display our results, which show that the fluctuations of central residues of SII are increased in K-Ras^{G12D}.

The correlated motions of residues are markedly increased in K-Ras^{G12D} in comparison to K-Ras^{WT}. Regulation of protein dynamics is strictly coordinated by the correlations of residue fluctuations. Figures 3C-D present pairwise correlations of residue fluctuations (C_{ij}), where we show the results for K-Ras^{WT} and K-Ras^{G12D} in the left and right panels, respectively. Specifically, β3-SII residues become negatively correlated with the residues of P-loop, SI, and β4-α3.

The characteristic decay times of residues in P-loop, SI and SII are longer in K-Ras^{G12D}. Fluctuations of each residue has a characteristic decay time that corresponds to the memory of its past[56]. In other words, characteristic decay time is the time-delay for which the present fluctuations of residue *i* becomes decoupled from its past fluctuations. Figure 3B shows that the characteristic decay times of residue fluctuations**.** Moreover, SII residues show the longest correlation decay times within the K-Ras^{G12D} residues.

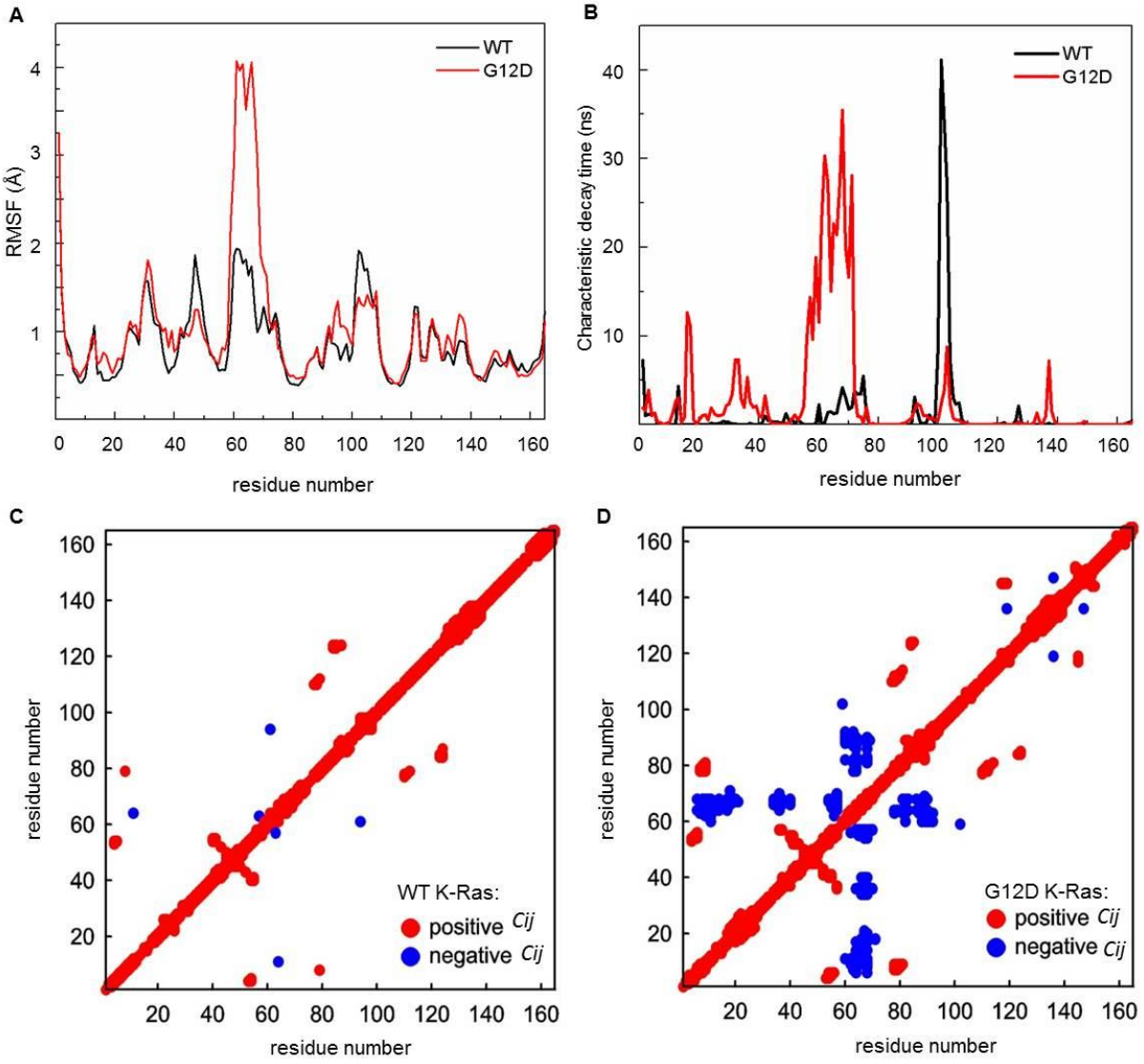

Figure 3. Dynamic changes in K-Ras upon G12D mutation. Residue indices 1-165 refer to K-Ras. (A) RMSF values of K-Ras^{WT} (black) and K-Ras^{G12D} (red) residues. (B) Characteristic decay times of residue fluctuations in K-Ras^{WT} (black) and K-Ras^{G12D} (red). (C-D) Correlation coefficient maps of K-Ras^{WT} (C) and K-Ras^{G12D} (D). Red dots show positive correlations and blue dots show negative correlations.

SII motions are the main drivers of correlated motions in K-Ras^{G12D}. We analyzed mutant K-Ras dynamics in depth by applying time-delayed correlation analysis to MD simulation data of K-Ras^{G12D}. The time-delayed correlation of residues *i* and *j* ($C_{ij}(\tau)$) is the correlation of the fluctuations of residue *i* with the later fluctuations of residue *j*. Through this analysis, we identified driver-responder residue pairs in K-Ras^{G12D} motions. Then, we compared the driver-responder pairs for K-Ras^{G12D} that we have calculated here with those for K-Ras^{WT} that we have previously published[45].

Our causality analysis calculations show that in K-Ras^{G12D}, the motions of SII are the main drivers, driving the motions of both P-loop and β3. We present the time delayed correlation plots of Q70 (SII) with V9 (P-loop) (Figure 4A) and C80 (β4) (Figure 4B) and D69 (SII) with

D54 (β3) (Figure 4C) for K-Ras^{G12D}. These are newly formed driver-responder interactions which do not exist in K-Ras^{WT}.

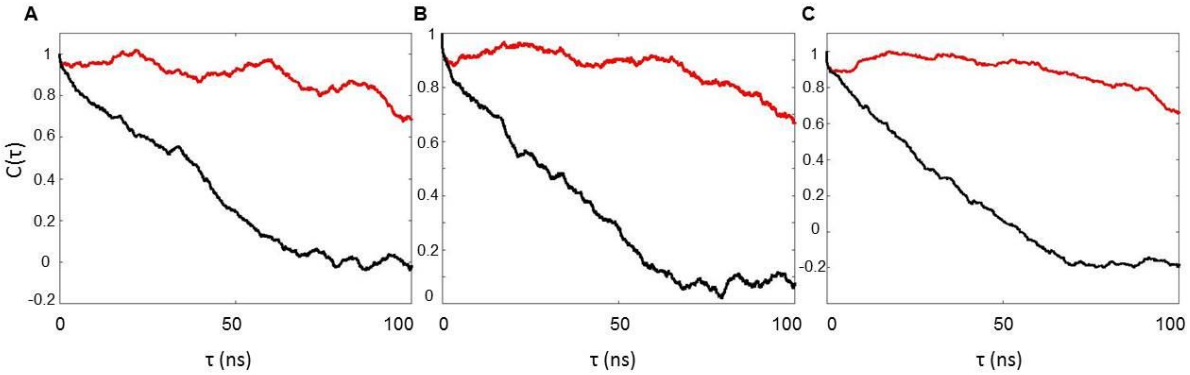

Figure 4.Causality relations in K-Ras^{G12D}. Red curves for $\langle \Delta R_i(t) \Delta R_j(t+\tau) \rangle$ show that the fluctuations of residue *i* at time *t* affect the fluctuations of residue *j* at a later time *t+τ*. X-axes represent t values from 1 ns to 100ns. All correlations ($C(\tau)$) are normalized with respect their value at zero ($C(0)$) and are shown in Y-axes. (A) Q70 (SII) fluctuations drive V9 (P-loop) fluctuations. (B) Q70 (SII) fluctuations drive C80 (β4) fluctuations. (C) D69 (SII) fluctuations drive D54 (β3) fluctuations.

Relations between the changes in K-Ras structure-conformation-dynamics

Formation of new salt bridges results in distortion of backbone Cα atoms in K-Ras^{G12D}. Our results show that upon K-Ras G12D mutation, salt bridges are formed between the sidechain atoms of the residues D12 (P-loop)-K16 (P-loop) and K16-D57 (SII). Furthermore, the SII region moves away from the P-loop, and they both move away from their neighbors. MD simulations of K-Ras^{G12D} show that the sidechains of the K16-D57 residue pair approach each other and form salt bridges, while their backbone Cα atoms move away from each other (Figure S1). Therefore, the new salt bridges formed between the P-loop and SII residues may cause the conformations of these two regions to move away from each other and from their neighbors. As a consequence of these structural and conformational changes in SII region, SII also moves away from SI and α3 regions.

Relationships Between Structural and Dynamic Changes in K-Ras^{G12D}. Since K-Ras^{G12D} simulations show the formation of a salt bridge between of D12 (P-loop) and K16 (P-loop), we investigated whether D12 and K16 moving closer due to the salt bridge causes changes in distal regions of K-Ras^{G12D}. For this purpose, we first defined a connectivity vector, $\Delta R_{12 \rightarrow 16}$, between D12 and K16 based on the definition in our previous paper[45], as summarized in Supplementary. We then defined connectivity vectors between the correlated residue pairs in K-Ras^{G12D}. Finally, we calculated the correlations of $\Delta R_{12 \rightarrow 16}$ with the other connectivity vectors. We discovered that that $\Delta R_{12 \rightarrow 16}$ is significantly correlated with $\Delta R_{60 \rightarrow 70}$, $\Delta R_{61 \rightarrow 75}$ and $\Delta R_{60 \rightarrow 82}$. Consequently, D12-K16 pair moving closer as a result of salt bridge formation affects the dynamics of distant residue pairs such as G60-Q70, Q61-G75 and G60-F82.

Relationships Between Conformational and Dynamic Changes in K-Ras^{G12D}

Fluctuations of dilated regions become negatively correlated in K-Ras^{G12D}. We observed that

after G12D mutation, negative correlations occur between the regions that move away from each other and from their neighbors. Combination of distance and correlation calculations gives us the relation between conformational and dynamic changes in the protein as a result of the mutation in its structure (Figure 5).

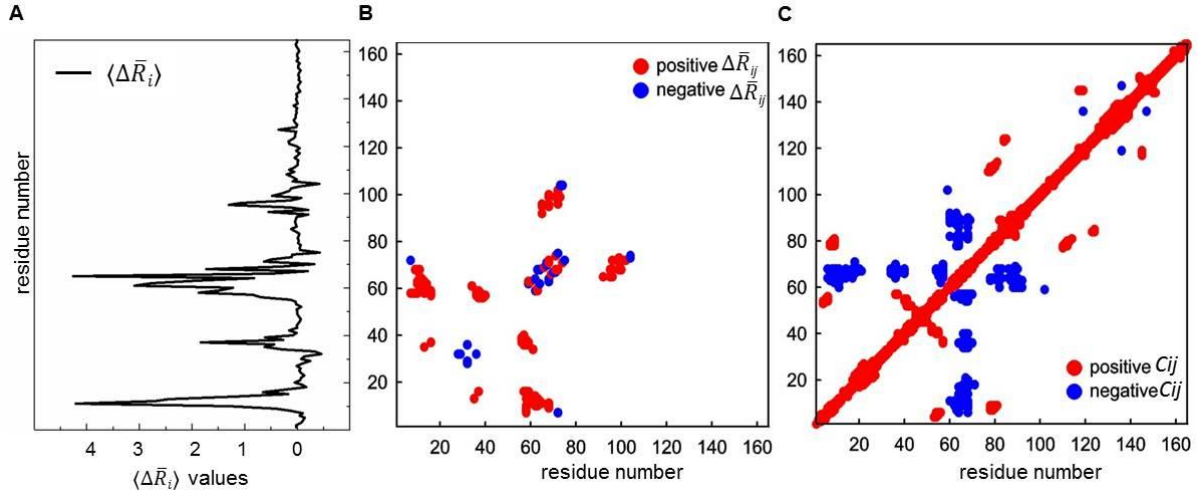

Figure 5. Comparison of the distance and correlation changes due to G12D mutation. (A) The average of all $\Delta\bar{R}_{ij}$ values for each residue, $\langle\Delta\bar{R}i\rangle$. (B) Difference of the average pairwise distances ($\Delta\bar{R}_{ij}$) (C) Pairwise correlation coefficients

Relationships Between Negative Correlations and Characteristic Decay Times in K-RaS^{G12D}. Our results show that upon K-Ras G12D mutation, the fluctuations of the SII region become negatively correlated with fluctuations of the P-loop, SI and α3 regions. Moreover, fluctuations of these regions have the longest correlation decay times in the protein (Figure 6). To investigate whether increased negative correlations between the residue fluctuations slow down the autocorrelation decay of the residue fluctuations, we calculated the average of negative correlation values for each residue of K-Ras^{G12D}. In Figure 7, we show that the residues whose fluctuations are more negatively correlated with other parts of the protein also have longer characteristic decay times.

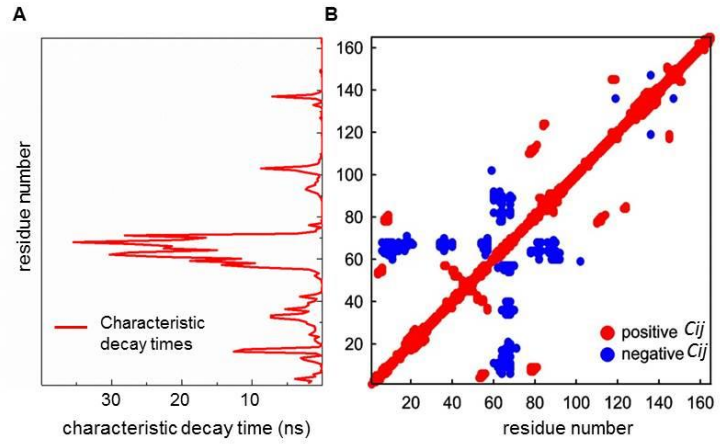

Figure 6. Comparison of characteristic decay times and pairwise correlatios in K-Ras^{G12D}. (A) Characteristic decay times of K-Ras^{G12D} residues. (B) Pairwise correlations in K-Ras^{G12D}.

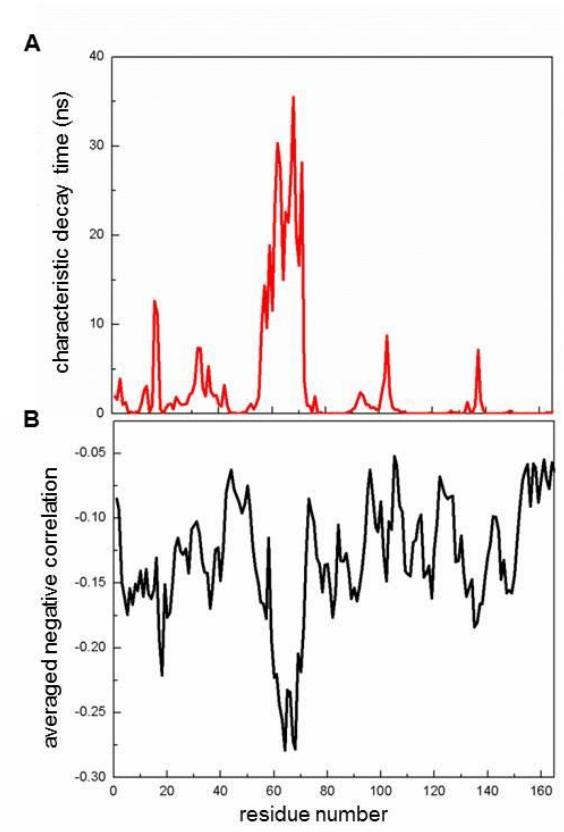

Figure 7. Comparison of characteristic decay times and averaged negative correlations in K-Ras^{G12D}. (A) Characteristic decay times of K-Ras^{G12D} residues. (B) Averaged negative correlation values per residue**.**

Relationships Between RMSF Values and Characteristic Decay Times in K-RAS^{G12D}. *Autocorrelations of residue fluctuations tend to decay slowly as fluctuation magnitudes increase.* Since our results showed that the residues in the SII region have the longest characteristic decay times and the greatest RMSF values, to investigate whether there is a correlation between these RMSF and autocorrelation decay time values, we plot RMSF vs. decay times per residue in Figure S3. Our results show that autocorrelation decay times become longer as fluctuations increase.

Relationships Between Negative Correlations, Characteristic Decay Times and Causality in K-RAS^{G12D}. *Negatively correlated residue pairs show causality.* All driver-responder residue pairs we identified in K-Ras^{G12D} correspond to regions that are negatively correlated during MD simulations.

Driver residues exhibit slow autocorrelation decays. A slow autocorrelation decay indicates that the residue has a strong memory of its past fluctuations. To compare the memory lengths of the residues in K-Ras^{G12D} driver-responder pairs, we plot their autocorrelation decay curves (Figure 8). These plots show slower decay in drivers than responders, suggesting that they have longer memory lengths.

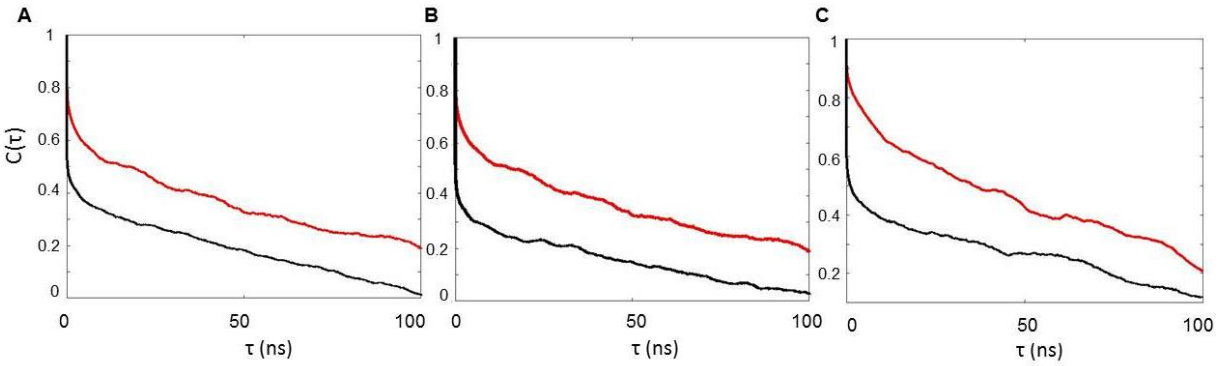

Figure 8. Autocorrelations for the fluctuations of the residues that are drivers or responders in K-Ras^{G12D}. Curves for $\langle \Delta R_i(t) \Delta R_i(t+\tau) \rangle$ show that fluctuations of residue *i* at time *t* affect its fluctuations at a later time *t+τ*. Red curves correspond to autocorrelations with slow decay. X axes is for t values from 1 ns to 100ns. (A) Autocorrelations of residues Q70(driver)-V9(responder). Red line is autocorrelation decay curve of residue Q70, black line is autocorrelation decay curve of residue V9. (B) Autocorrelations of residues Q70(driver)-C80(responder). Red line is autocorrelation decay curve of residue Q70, black line is autocorrelation decay curve of residue C80. (C) Autocorrelations of residues D69(driver)-D54(responder). Red line is autocorrelation decay curve of residue D69, black line is autocorrelation decay curve of residue D54.

DISCUSSION

K-Ras is an important GTPase in cellular signaling, and is only active in its GTP-bound state[8,9]. Structurally, in active K-Ras, the P-loop, SI and SII regions are bound to the phosphate groups of GTP and are responsible for its GTPase function. However, when there is a G12D mutation in the P-loop, GTP hydrolysis is impaired and K-Ras freezes in its active state[9], causing uncontrollable cellular growth and evasion of apoptotic signals[24,57,58]. In order to quantify the conformational and dynamic changes caused by the G12D mutation, we followed a new integrated MD data analysis approach. Our method enabled us to relate the structural and conformational changes in the residues of a protein to changes in the regulation of the protein's dynamics. Using our method, we first discovered that the G12D mutation causes the formation of new salt bridges between the residues of K-Ras, which alter the conformations of those at the active site and α3, potentially affecting GTP hydrolysis, and freezing K-Ras in its active state. We then correlated the conformational changes in the residues at the active site and α3 to the dynamic changes in these regions. Our results show that the motions of SII become coupled to the motions of other residues at the active site and α3.

Next, to understand the time-dependent regulation of K-Ras^{G12D} motions, we measured the 'memory length' of each residue, and discovered that residues whose motions show strong coupling to the rest of the protein have a longer memory of their past. Specifically, the fluctuations of SII residues show the highest negative correlations with other parts of the protein and have the strongest memory. Most importantly, our results reveal the regulatory mechanism of K-Ras^{G12D} dynamics, where not only the residues in SII exhibit correlated fluctuations with other residues, they also drive them. These memory lengths of the residues

determine their driver-responder roles, and our results show that among all residues, those on SII have the strongest memory and are drivers in driver-responder pairs.

In this study, our first important finding is that the broad distribution of Q61-P-loop distances affects GTP hydrolysis function of K-Ras^{G12D}. Because in the G12D mutation, glycine residue is substituted by aspartate, which has a bulkier side group, it causes a structural change in the P-loop which affects the conformations of the other active site regions SI and SII, as observed in previous studies[22-24,59]. Our distance calculations show that after G12D mutation, the P-loop residues 11, 12, 13 move away from SII residue Q61. Moreover, the distances between Q61-A11, Q61-G12D and Q61-G13 display broad distributions (Figure 2). Since Q61 is a known catalytic residue that plays a critical role in both intrinsic and GAP-mediated GTP hydrolysis[10], the highly variable nature of the P-loop-Q61 distance may affect the GTP hydrolysis in K-Ras^{G12D}. Furthermore, our distance calculations also show that the residues in SII move away from some of the residues in SI, and α3, and distances between those residue pairs also display broad distributions in K-Ras^{G12D} (Figure 2). Considering the increased fluctuations of SII, these broad distance distributions with larger peak values between SII and the other parts of the protein may be arising from the increased flexibility of SII in K-Ras^{G12D}.

Our second important finding is that the residue E37 moves away from residue D57 in K-Ras^{G12D} and alters Raf effector protein binding. The residues E37 and D57 are known hot-spots for the interaction of K-Ras with Raf[60]. This interaction has been previously shown to be impaired upon G12D mutation[61,62]. Our distance analyses describe the possible reason for this impartment is that these two hot-spot residues move away from each other and their neighbors in K-Ras^{G12D}.

Third, residues R73 and K104 move closer upon mutation and alter PI3Kγ effector binding. Pairwise distance calculations indicate that the distances of residue pairs 63-68, 72-75 and 73-104 significantly decrease upon G12D mutation. The 73-104 pair is particularly important since R73 is critical for interaction with the effector protein PI3Kγ[63]. Experiments have shown that PI3Kγ is preferably activated by K-Ras^{G12D} with higher binding affinity[61,62]. Additionally, the backbone carbonyls of R73 interact with the amino sidechain of K104[64]. Therefore, the decreased distance between R73 and K104 in K-Ras^{G12D} (Figure 2D) may affect the interaction of these residues that allow PI3Kγ binding with higher affinity.

Fourth, active site residues that move apart in K-Ras^{G12D} may alter its GTPase function. K-Ras undergoes conformational changes when it binds to GTP. The P-loop, SI and SII constitute the active site of the protein that binds to phosphate groups of GTP and participates in GTP hydrolysis[10]. SI and SII are also responsible for controlling the binding to effector molecules. Conformational changes in the active site affect K-Ras interactions with the GAPs which amplify the GTPase activity of K-Ras[65]. Our distance calculations showed that the active site residues of K-Ras^{G12D} move away from their neighbors (Figure 1C) due to the structural change in the P-loop. SII fluctuations also increase (Figure 3A). These observations are consistent with previous studies that showed that the larger distances between active site residues and increased SII fluctuations in K-Ras^{G12D}[24]. Since conformations of the active site play important roles in GTPase activity of K-Ras and its binding ability to GAPs, we postulate that the deviation of active site residues may impair the GTP hydrolysis and also GAP binding ability which leads to the constitutively active K-Ras^{G12D}.

And fifth, G12D mutation augments the correlations between SII and the regions by increasing the flexibility of SII. As seen in the pairwise correlation maps, K-Ras^{G12D} differs markedly from K-Ras^{WT} and displays increased correlations between the fluctuations of SII residues and other parts of the protein. This is consistent the increased amplitude of the SII fluctuations in K-Ras^{G12D}, as shown in Figure 3. These results are consistent with a previous study that showed that SII fluctuations display increased level of fluctuations and negative correlations[24].

Overall, our results provide a mechanistic understanding of the dynamic regulatory mechanisms of K-Ras^{G12D} as well as predictions of sites that regulate its motions (such as SII). Targeting these sites with small molecules can be an effective strategy for the allosteric inhibition of oncogenic K-Ras^{G12D} for the treatment of several cancers.

REFERENCES

1 Stephen, A. G., Esposito, D., Bagni, R. K. & McCormick, F. Dragging ras back in the ring. *Cancer Cell* **25**, 272-281, doi:10.1016/j.ccr.2014.02.017 (2014).

2 Forbes, S. A. *et al.* COSMIC: exploring the world's knowledge of somatic mutations in human cancer. *Nucleic Acids Res* **43**, D805-811, doi:10.1093/nar/gku1075 (2015).

3 Prior, I. A., Lewis, P. D. & Mattos, C. A comprehensive survey of Ras mutations in cancer. *Cancer Res* **72**, 2457-2467, doi:10.1158/0008-5472.CAN-11-2612 (2012).

4 Pao, W. *et al.* KRAS mutations and primary resistance of lung adenocarcinomas to gefitinib or erlotinib. *Plos Med* **2**, 57-61, doi:ARTN e17 10.1371/journal.pmed.0020017 (2005).

5 Amado, R. G. *et al.* Wild-type KRAS is required for panitumumab efficacy in patients with metastatic colorectal cancer. *J Clin Oncol* **26**, 1626-1634, doi:10.1200/JCO.2007.14.7116 (2008).

6 Lievre, A. *et al.* KRAS mutation status is predictive of response to cetuximab therapy in colorectal cancer. *Ann Oncol* **17**, 42-42 (2006).

7 Herrmann, C. & Nassar, N. Ras and its effectors. *Prog Biophys Mol Biol* **66**, 1-41 (1996).

8 Milburn, M. V. *et al.* Molecular Switch for Signal Transduction - Structural Differences between Active and Inactive Forms of Protooncogenic Ras Proteins. *Science* **247**, 939-945, doi:DOI 10.1126/science.2406906 (1990).

9 Vetter, I. R. & Wittinghofer, A. Signal transduction - The guanine nucleotide-binding switch in three dimensions. *Science* **294**, 1299-1304, doi:10.1126/science.1062023 (2001).

10 Lu, S. *et al.* Ras Conformational Ensembles, Allostery, and Signaling. *Chem Rev* **116**, 6607-6665, doi:10.1021/acs.chemrev.5b00542 (2016).

11 Glennon, T. M., Villa, J. & Warshel, A. How does GAP catalyze the GTPase reaction of Ras?: A computer simulation study. *Biochemistry* **39**, 9641-9651, doi:DOI 10.1021/bi000640e (2000).

12 Scheffzek, K. *et al.* The Ras-RasGAP complex: Structural basis for GTPase activation and its loss in oncogenic Ras mutants. *Science* **277**, 333-338, doi:DOI 10.1126/science.277.5324.333 (1997).

13 Schubbert, S., Shannon, K. & Bollag, G. Hyperactive Ras in developmental disorders and cancer. *Nat Rev Cancer* **7**, 295-308, doi:10.1038/nrc2109 (2007).

14 Smith, M. J., Neel, B. G. & Ikura, M. NMR-based functional profiling of RASopathies and oncogenic RAS mutations. *Proc Natl Acad Sci U S A* **110**, 4574-4579, doi:10.1073/pnas.1218173110 (2013).

15 Adjei, A. A. Blocking oncogenic Ras signaling for cancer therapy. *J Natl Cancer Inst* **93**, 1062-1074 (2001).

16 Malumbres, M. & Barbacid, M. RAS oncogenes: the first 30 years. *Nat Rev Cancer* **3**, 459-465, doi:10.1038/nrc1097 (2003).
17 McCormick, F. K-Ras protein as a drug target. *J Mol Med (Berl)* **94**, 253-258, doi:10.1007/s00109-016-1382-7 (2016).
18 Lu, S., Jang, H., Gu, S., Zhang, J. & Nussinov, R. Drugging Ras GTPase: a comprehensive mechanistic and signaling structural view. *Chem Soc Rev* **45**, 4929-4952, doi:10.1039/c5cs00911a (2016).
19 Ostrem, J. M. & Shokat, K. M. Direct small-molecule inhibitors of KRAS: from structural insights to mechanism-based design. *Nat Rev Drug Discov*, doi:10.1038/nrd.2016.139 (2016).
20 Marcus, K. & Mattos, C. Direct Attack on RAS: Intramolecular Communication and Mutation-Specific Effects. *Clin. Cancer Res.* **21**, 1810-1818, doi:10.1158/1078-0432.ccr-14-2148 (2015).
21 Prakash, P., Zhou, Y., Liang, H., Hancock, J. F. & Gorfe, A. A. Oncogenic K-Ras Binds to an Anionic Membrane in Two Distinct Orientations: A Molecular Dynamics Analysis. *Biophysical Journal* **110**, 1125-1138, doi:10.1016/j.bpj.2016.01.019 (2016).
22 Lu, S. Y., Jang, H., Nussinov, R. & Zhang, J. The Structural Basis of Oncogenic Mutations G12, G13 and Q61 in Small GTPase K-Ras4B. *Sci Rep-Uk* **6**, doi:ARTN 21949 10.1038/srep21949 (2016).

23 Prakash, P., Hancock, J. F. & Gorfe, A. A. Binding hotspots on K-ras: consensus ligand binding sites and other reactive regions from probe-based molecular dynamics analysis. *Proteins* **83**, 898-909, doi:10.1002/prot.24786 (2015).
24 Chen, C. C. *et al.* Computational analysis of KRAS mutations: implications for different effects on the KRAS p.G12D and p.G13D mutations. *PLoS One* **8**, e55793, doi:10.1371/journal.pone.0055793 (2013).
25 Patricelli, M. P. *et al.* Selective Inhibition of Oncogenic KRAS Output with Small Molecules Targeting the Inactive State. *Cancer Discov* **6**, 316-329, doi:10.1158/2159-8290.CD-15-1105 (2016).
26 Ostrem, J. M., Peters, U., Sos, M. L., Wells, J. A. & Shokat, K. M. K-Ras(G12C) inhibitors allosterically control GTP affinity and effector interactions. *Nature* **503**, 548-+, doi:10.1038/nature12796 (2013).
27 Lim, S. M. *et al.* Therapeutic targeting of oncogenic K-Ras by a covalent catalytic site inhibitor. *Angew Chem Int Ed Engl* **53**, 199-204, doi:10.1002/anie.201307387 (2014).
28 Singh, H., Longo, D. L. & Chabner, B. A. Improving Prospects for Targeting RAS. *Journal of Clinical Oncology* **33**, 3650-+, doi:10.1200/Jco.2015.62.1052 (2015).
29 Grant, B. J. *et al.* Novel Allosteric Sites on Ras for Lead Generation. *Plos One* **6**, doi:ARTN e25711 10.1371/journal.pone.0025711 (2011).

30 Leshchiner, E. S. *et al.* Direct inhibition of oncogenic KRAS by hydrocarbon-stapled SOS1 helices. *Proceedings of the National Academy of Sciences of the United States of America* **112**, 1761-1766, doi:10.1073/pnas.1413185112 (2015).
31 Lito, P., Solomon, M., Li, L. S., Hansen, R. & Rosen, N. Allele-specific inhibitors inactivate mutant KRAS G12C by a trapping mechanism. *Science* **351**, 604-608, doi:10.1126/science.aad6204 (2016).
32 Jang, H. *et al.* Mechanisms of membrane binding of small GTPase K-Ras4B farnesylated hypervariable region. *J Biol Chem* **290**, 9465-9477, doi:10.1074/jbc.M114.620724 (2015).
33 Jang, H. *et al.* The higher level of complexity of K-Ras4B activation at the membrane. *Faseb J* **30**, 1643-1655, doi:10.1096/fj.15-279091 (2016).
34 Scarabelli, G. & Grant, B. J. Kinesin-5 allosteric inhibitors uncouple the dynamics of nucleotide, microtubule, and neck-linker binding sites. *Biophys J* **107**, 2204-2213, doi:10.1016/j.bpj.2014.09.019 (2014).

35 Kumar, A., Glembo, T. J. & Ozkan, S. B. The Role of Conformational Dynamics and Allostery in the Disease Development of Human Ferritin. *Biophys J* **109**, 1273-1281, doi:10.1016/j.bpj.2015.06.060 (2015).

36 Alred, E. J., Scheele, E. G., Berhanu, W. M. & Hansmann, U. H. Stability of Iowa mutant and wild type Abeta-peptide aggregates. *J Chem Phys* **141**, 175101, doi:10.1063/1.4900892 (2014).

37 Gkeka, P. *et al.* Investigating the structure and dynamics of the PIK3CA wild-type and H1047R oncogenic mutant. *PLoS Comput Biol* **10**, e1003895, doi:10.1371/journal.pcbi.1003895 (2014).

38 Lu, S. *et al.* The Mechanism of ATP-Dependent Allosteric Protection of Akt Kinase Phosphorylation. *Structure* **23**, 1725-1734, doi:10.1016/j.str.2015.06.027 (2015).

39 Blacklock, K. & Verkhivker, G. M. Computational modeling of allosteric regulation in the hsp90 chaperones: a statistical ensemble analysis of protein structure networks and allosteric communications. *PLoS Comput Biol* **10**, e1003679, doi:10.1371/journal.pcbi.1003679 (2014).

40 Sun, H. *et al.* Revealing the favorable dissociation pathway of type II kinase inhibitors via enhanced sampling simulations and two-end-state calculations. *Sci Rep* **5**, 8457, doi:10.1038/srep08457 (2015).

41 Sliwoski, G., Kothiwale, S., Meiler, J. & Lowe, E. W., Jr. Computational methods in drug discovery. *Pharmacol Rev* **66**, 334-395, doi:10.1124/pr.112.007336 (2014).

42 Stank, A., Kokh, D. B., Fuller, J. C. & Wade, R. C. Protein Binding Pocket Dynamics. *Acc Chem Res* **49**, 809-815, doi:10.1021/acs.accounts.5b00516 (2016).

43 Borhani, D. W. & Shaw, D. E. The future of molecular dynamics simulations in drug discovery. *J Comput Aided Mol Des* **26**, 15-26, doi:10.1007/s10822-011-9517-y (2012).

44 Durrant, J. D. & McCammon, J. A. Molecular dynamics simulations and drug discovery. *BMC Biol* **9**, 71, doi:10.1186/1741-7007-9-71 (2011).

45 Vatansever, S., Gumus, Z. H. & Erman, B. Intrinsic K-Ras dynamics: A novel molecular dynamics data analysis method shows causality between residue pair motions. *Sci Rep* **6**, 37012, doi:10.1038/srep37012 (2016).

46 Discovery Studio Modeling Environment v. Release 4.5 (San Diego: Dassault Systèmes, 2015).

47 Phillips, J. C. *et al.* Scalable molecular dynamics with NAMD. *Journal of Computational Chemistry* **26**, 1781-1802, doi:10.1002/jcc.20289 (2005).

48 Hornak, V. *et al.* Comparison of multiple amber force fields and development of improved protein backbone parameters. *Proteins-Structure Function and Bioinformatics* **65**, 712-725, doi:10.1002/prot.21123 (2006).

49 Wang, J. M., Wolf, R. M., Caldwell, J. W., Kollman, P. A. & Case, D. A. Development and testing of a general amber force field. *Journal of Computational Chemistry* **25**, 1157-1174, doi:DOI 10.1002/jcc.20035 (2004).

50 Humphrey, W., Dalke, A. & Schulten, K. VMD: Visual molecular dynamics. *J Mol Graph Model* **14**, 33-38, doi:Doi 10.1016/0263-7855(96)00018-5 (1996).

51 Bahar, I., Atilgan, A. R. & Erman, B. Direct evaluation of thermal fluctuations in proteins using a single-parameter harmonic potential. *Fold Des* **2**, 173-181, doi:Doi 10.1016/S1359-0278(97)00024-2 (1997).

52 Haliloglu, T., Bahar, I. & Erman, B. Gaussian dynamics of folded proteins. *Physical Review Letters* **79**, 3090-3093, doi:DOI 10.1103/PhysRevLett.79.3090 (1997).

53 Bahar, I., Atilgan, A. R., Demirel, M. C. & Erman, B. Vibrational dynamics of folded proteins: Significance of slow and fast motions in relation to function and stability. *Physical Review Letters* **80**, 2733-2736, doi:DOI 10.1103/PhysRevLett.80.2733 (1998).

54 Atilgan, A. R., Akan, P. & Baysal, C. Small-world communication of residues and significance for protein dynamics. *Biophys J* **86**, 85-91, doi:10.1016/S0006-3495(04)74086-2 (2004).

55 Woodcock, L. V. Entropy difference between the face-centred cubic and hexagonal close-packed crystal structures. *Nature* **385**, 141-143, doi:DOI 10.1038/385141a0 (1997).
56 Okan, O. B., Atilgan, A. R. & Atilgan, C. Nanosecond motions in proteins impose bounds on the timescale distributions of local dynamics. *Biophys J* **97**, 2080-2088, doi:10.1016/j.bpj.2009.07.036 (2009).
57 Downward, J. Targeting ras signalling pathways in cancer therapy. *Nature Reviews Cancer* **3**, 11-22, doi:10.1038/nrc969 (2003).
58 Lu, S. *et al.* GTP Binding and Oncogenic Mutations May Attenuate Hypervariable Region (HVR)-Catalytic Domain Interactions in Small GTPase K-Ras4B, Exposing the Effector Binding Site. *J Biol Chem* **290**, 28887-28900, doi:10.1074/jbc.M115.664755 (2015).
59 Lu, S. Y. *et al.* GTP Binding and Oncogenic Mutations May Attenuate Hypervariable Region (HVR)-Catalytic Domain Interactions in Small GTPase K-Ras4B, Exposing the Effector Binding Site. *Journal of Biological Chemistry* **290**, 28887-28900, doi:10.1074/jbc.M115.664755 (2015).
60 Baussand, J. & Kleinjung, J. Specific Conformational States of Ras GTPase upon Effector Binding. *J Chem Theory Comput* **9**, 738-749, doi:10.1021/ct3007265 (2013).
61 Biochemical and Structural Analysis of Common Cancer-Associated KRAS Mutations. (2015).
62 Ihle, N. T. *et al.* Effect of KRAS Oncogene Substitutions on Protein Behavior: Implications for Signaling and Clinical Outcome. *J Natl Cancer I* **104**, 228-239, doi:10.1093/jnci/djr523 (2012).
63 Castellano, E. & Downward, J. RAS Interaction with PI3K: More Than Just Another Effector Pathway. *Genes Cancer* **2**, 261-274, doi:10.1177/1947601911408079 (2011).
64 Yin, G. *et al.* A KRAS GTPase K104Q Mutant Retains Downstream Signaling by Offsetting Defects in Regulation. *J Biol Chem* **292**, 4446-4456, doi:10.1074/jbc.M116.762435 (2017).
65 Lu, S., Jang, H., Zhang, J. & Nussinov, R. Inhibitors of Ras-SOS Interactions. *ChemMedChem* **11**, 814-821, doi:10.1002/cmdc.201500481 (2016).